

Emergent BCS regime of the two-dimensional fermionic Hubbard model: ground-state phase diagram

YOUJIN DENG^{1,2} (a), EVGENY KOZIK^{3,4} (b), NIKOLAY V. PROKOF'EV^{2,5} and BORIS V. SVISTUNOV^{1,2,5}

¹ Hefei National Laboratory for Physical Sciences at Microscale, Department of Modern Physics, and Synergetic Innovation Center of Quantum Information and Quantum Physics, University of Science and Technology of China-Hefei, Anhui 230026, China

² Department of Physics, University of Massachusetts-Amherst, MA 01003, USA

³ Department of Physics, King's College London, Strand-London WC2R 2LS, UK

⁴ Centre de Physique Théorique, Ecole Polytechnique, CNRS-91128 Palaiseau Cedex, France

⁵ Russian Research Center "Kurchatov Institute," 123182 Moscow, Russia

PACS 71.10.Fd – Lattice fermion models (Hubbard model, etc.)
 PACS 02.70.Ss – Quantum Monte Carlo methods
 PACS 74.20.Fg – BCS theory and its development

Abstract – For over half a century, the Hubbard model has played a paradigmatic role in attempts to understand quantum phenomena exhibited by correlated electrons in solids. Despite substantial effort and apparent simplicity of the model, its behavior in many important regimes has remained unknown. Here we study superfluidity in the two-dimensional Hubbard model with controlled error bars up to the coupling strength $U = 4$ and filling factor $n = 0.7$. We show, by means of unbiased diagrammatic Monte Carlo simulations, that in this regime the superfluid transition is governed by Fermi liquid physics with an emergent weak BCS-type coupling driving the instability. The corresponding ground-state phase diagram in the (n, U) plane describes competition between the superfluid states of p - and d -wave symmetry. We also report dimensionless coupling constants in this effective BCS regime.

The fermionic Hubbard model [1, 2],

$$\hat{H} = - \sum_{\langle i, j \rangle, \sigma} \hat{c}_{i\sigma}^\dagger \hat{c}_{j\sigma} + U \sum_i \hat{n}_{i\uparrow} \hat{n}_{i\downarrow} - \mu \sum_{i, \sigma} \hat{n}_{i\sigma} \quad (1)$$

($\hat{c}_{i\sigma}^\dagger$ creates a fermion with spin projection $\sigma = \uparrow, \downarrow$ on site i ; $\hat{n}_{i\sigma} = \hat{c}_{i\sigma}^\dagger \hat{c}_{i\sigma}$; $\langle \dots \rangle$ restricts summation to neighboring lattice sites; U and μ are, respectively, the on-site repulsion and the chemical potential in units of the hopping amplitude) is one of “standard models” of condensed matter physics. The metal-insulator transition at half filling $\langle \hat{n}_{i\uparrow} + \hat{n}_{i\downarrow} \rangle = 1$, along with the antiferromagnetism promoted by it, was the main context of the original formulation of (1) and subsequent two decades of its intensive theoretical studies. The advent of high-temperature superconductivity dramatically enhanced (and changed the focus of) the interest to Eq. (1). It became paradigmatic

for high-temperature superconductors [2], *at least* as a minimalistic Hamiltonian featuring (not far from half filling) the relevant $d_{x^2-y^2}$ Cooper instability, solely due to repulsive interaction between fermions. The most recent wave of interest to Eq. (1) has been generated by its direct realization with ultracold atoms in optical lattices [3–5].

Decades of theoretical studies of Cooper instability in the model (1) have seen a number of remarkable successes. Controlled results were obtained in certain limiting cases: vanishingly small interaction or/and low filling [6–13] and close to half-filling, by a combination of numerical methods including determinant Monte Carlo [14–16], density matrix renormalization group [17], and the dynamical mean-field theory on large clusters [18–27]. For the 2D case we are interested in here, it has been found that, at a fixed filling factor and $U \rightarrow 0$ (within the second-order perturbation theory in U) the ground state of the system is either d_{xy} -wave (smaller fillings) or $d_{x^2-y^2}$ -wave (higher fillings) BCS superfluid, with a

(a) yjdeng@ustc.edu.cn

(b) evgeny.kozik@kcl.ac.uk

pocket of a p -wave phase near quarter filling [13]. It has been also shown that, in the low-density limit at any fixed U , the ground state of the system is the p -wave BCS superfluid [9]. The dynamic-cluster-approximation (DCA) simulations revealed (see [27] and references therein) a region of high-temperature $d_{x^2-y^2}$ -wave pairing developing at $U \gtrsim 6$. Nevertheless, the rich ground-state phase diagram guaranteed by the above-mentioned findings remains elusive: So far, *none* of the phase boundaries is known.

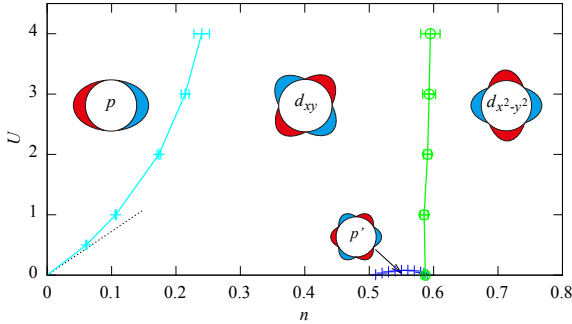


Fig. 1: Ground-state phase boundaries of the fermionic Hubbard model (1) in the emergent BCS regime. (Classification of superfluid phases in terms of the D_{4h} group is explained in the text.) The dashed straight line shows the $U \rightarrow 0$ limit

$$n_c(U) = 0.139U \text{ for the } p\text{-}d_{xy} \text{ phase boundary. The } p' \text{ phase with six nodes exists only up to } U \approx 0.08.$$

Results. —We report accurate controllable results for a significant part of the ground-state phase diagram (Fig. 1) of the Hubbard model, Eq. (1), on the square lattice. We concentrate on the region of moderate bare coupling $U \leq 4$ and filling $n < 0.7$, and first observe that there the system exhibits Landau Fermi-liquid behavior at temperatures $T_c < T \ll E_F$; i.e., between the Fermi energy E_F and the temperature of the superfluid phase transition $T_c \ll E_F$. Hence we employ the first-principles theoretical framework consisting of: (i) asymptotically exact (in the $T_c/E_F \rightarrow 0$ limit) diagrammatic theory of Cooper instability in the Fermi liquid state [28, 29] and (ii) unbiased Bold diagrammatic Monte Carlo (BDMC) simulation of the Fermi liquid parameters. We base our BDMC approach on the skeleton expansion in terms of the fully dressed interaction vertex in the particle-particle channel (analogous to the continuous-space technique developed in Refs. [30, 31] for the resonant Fermi gas) with an additional trick leading to near cancellation of large-amplitude contributions in the interaction vertex to improve numerical efficiency. In the considered regime of $U \leq 4$, $n < 0.7$, the skeleton series is known to produce exact results [32], which we also checked explicitly by benchmarking the Green’s function against the corresponding bare-series calculation. The approach allows us to controllably address all system’s properties in the Landau Fermi-liquid regime at temperatures $T_c < T \ll E_F$ and deduce the leading channel for Cooper instability.

Our main qualitative finding is that the effective (dimensionless) couplings in the Cooper channel remain small (≤ 0.1) up to essentially non-perturbative values of the bare coupling $U \sim 4$ and densities up to $n < 0.7$. This makes the problem of development of the Cooper instability amenable to controlled analytic treatment by diagrammatic perturbation theory. However, accurately determining the small effective coupling constants, shown in Fig. 2, up to $U = 4$ requires a dramatic effort, involving development of essentially non-perturbative numeric techniques, such as a variant of BDMC employed here, and substantial computation time (see a discussion in the following section).

The revealed ground-state phase diagram is shown in Fig. 1—where the error bars on the phase boundaries represent the full (systematic and statistical) error—and discussed in detail below.

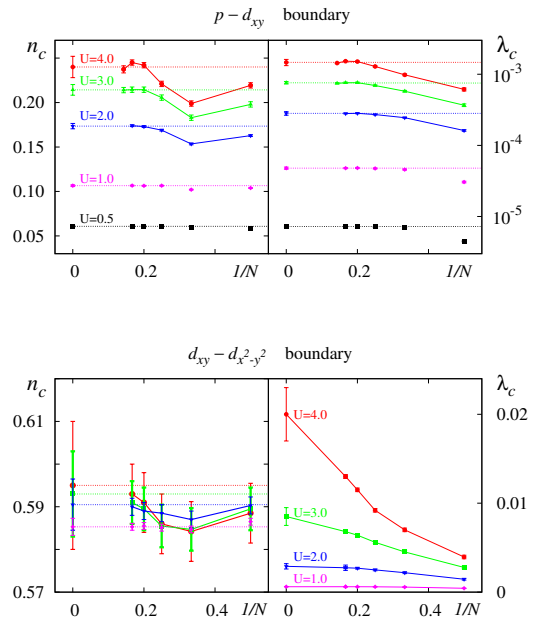


Fig. 2: Critical density and dimensionless coupling constants as functions of maximum diagram order, N , at various points along the phase boundaries (parameterized by U) with extrapolation to the $N \rightarrow \infty$ limit. Extrapolation was based on linear fits to the last three points. Error bars were deduced from the stability of results when fits included four points.

Discussion. —Let us first focus on the lower left corner ($U \rightarrow 0$, $n \rightarrow 0$ limit) in Fig. 1, which has been extensively studied by the perturbation theory in the $n \rightarrow 0$ and $U \rightarrow 0$ limit in Refs. [7–9]. Our p - d_{xy} phase boundary is consistent with the linear law, $n_c = 0.139U$, shown by the dashed line. This behavior is understood by comparing effective coupling constants derived in Refs. [7, 8] ($\propto U^2$) and in Ref. [9] ($\propto U^3$). [The prediction for the slope from Refs. [7–9] would be a factor of two smaller, $n_c/U = 0.069$.

We attribute the discrepancy to typos: Factors of two were missing in the density of states or/and the Cooper channel wave functions normalization.]

The phase diagram in the limit of $U \rightarrow 0$ for all densities n has been obtained in second-order in U calculations of Refs. [13, 35]. For $0.5 < n < 0.6$ the p -wave state is rather peculiar; we denote it p' to emphasize the difference from the conventional p -wave, which was not fully addressed in Ref. [13]. In a p -wave superfluid, the wavefunction of Cooper pairs has two nodes, in direct analogy with the case of the continuous rotation group (justifying the usage of the same symbol p). In contrast, the pairing wavefunction of the p' -phase features six nodes [34].

Raghu *et al.* [35] generalized the second-order perturbation theory developed in Ref. [13] to other types of lattices. However, in contrast to Ref. [13], the p' state at $0.5 < n < 0.6$ is apparently absent from their results for the square lattice. Apart from creating a controversy, the discrepancy circumstantially suggests that this part of the phase diagram might be very sensitive even at $U < 1$. This is indeed the case revealed here: the pocket of the p' phase at $0.5 < n < 0.6$ vanishes already at $U \gtrsim 0.08$, as shown in Fig. 1. Our calculations also demonstrate that the BCS coupling constants λ reported in Ref. [35] are overestimated by a factor of $1/\rho$, where ρ is the Fermi-surface density of states, taking the values $1/4\pi \leq \rho \lesssim 0.185$ for $0 \leq n \lesssim 0.8$. This implies that from Ref. [35] one can wrongly conclude that the superfluid T_c , which is exponentially sensitive to λ ($T_c \sim E_F \exp(-1/\lambda)$) is orders of magnitude larger than it actually is, suggesting realization of high-temperature superconductivity by the Hubbard model already at very moderate U .

In general, our calculations reveal that perturbative $U \rightarrow 0$ results cannot be used to reasonably estimate the actual BCS coupling constants λ (and thus the corresponding T_c). Already for a weak interaction $U = 1$, the values of λ at the ($d_{xy} - d_{x^2-y^2}$) boundary computed up to terms $\propto U^3$ are larger than those computed up to U^2 by a factor between two and three.

Even by state-of-the-art numeric techniques it still remains challenging to accurately and reliably compute basic physical quantities for the Hubbard model in the weak-to-intermediate coupling regime of $U \lesssim 4$. For instance, for ($U = 2, n = 0.8, T = 0.25$) dynamical-cluster-approximation results display significant oscillatory behavior as a function of the cluster size L up to $L = 98$ lattice sites, and thus accurate extrapolation to the thermodynamic limit $L \rightarrow \infty$ becomes difficult [36]. Within the BDMC framework, one has to go substantially beyond the second-order *skeleton* diagrams—convergence is observed only after accounting for diagrams of order $N = 5$ (in terms of the fully dressed interaction vertex in the particle-particle channel and not the bare U) and above. Our scheme of combining BDMC and semi-analytic BCS treatment provides an effective and controllable method for studying correlated fermionic systems in the emergent BCS regime. The present calculation can be immediately

generalized to other lattices or higher spatial dimensions, and, with minor modifications, can be used to explore other phase boundaries such as the antiferromagnetic transition [37, 38].

Our most unexpected and essentially non-perturbative result here is the near-vertical boundary between different d -wave states at $n \approx 0.6$, see Fig. 1. This behavior has nothing to do with the perturbation theory because (i) the boundary *terminates* at the p' lobe at $U \approx 0.08$ (see Fig. 1) implying that the $U \rightarrow 0$ theory fails at $U \approx 0.08$ already, and (ii) the effective coupling λ along the boundary has strong dependence on U and the diagram order, see the lower right panel in Fig. 2.

Finally, we emphasize that in the $d_{x^2-y^2}$ phase, the dimensionless BCS coupling $\lambda_{d_{x^2-y^2}}$ increases rapidly as the particle density n and bare interaction U are increased. At the upper right corner of Fig. 1, ($U = 4, n = 0.7$), one already has $\lambda_{d_{x^2-y^2}} \sim 0.1$ corresponding to a critical temperature $T_c/E_F \sim 5 \times 10^{-5}$, typical for conventional superconductors. This is still well within the domain of the emergent BCS regime, but if $\lambda_{d_{x^2-y^2}}$ increases further by 50% at larger U and n , the system would meet the criterion for being a high-temperature superconductor. As Fig. 2 suggests, the value of λ may indeed be significantly enhanced as U is further increased from $U = 4$. Unfortunately, the present BDMC formulation fails in such strongly correlated regime [32], and novel techniques/approaches dealing with diagrammatic series need to be developed [22, 23]. Nevertheless, even within the present approach, by computing $T_c(n, U)$ (with correct pre-exponential factor [39, 40]) up to the ($U = 4, n = 0.7$) corner, one can obtain a reasonable extrapolation to the intriguing region of ($U \approx 6, n \approx 0.85$) thus shedding a significant light on the crossover from emergent BCS to high- T_c regime expected to take place in this range of parameters [27].

Methods. —The *emergent BCS regime* is a Cooper instability due to weak effective attraction between the quasiparticles developing in a strongly correlated fermionic system at energy scales much smaller than the Fermi energy. In this scenario, as the temperature is decreased, the system first enters the standard Fermi liquid (FL) state characterized by renormalized quasiparticle properties and effective interactions. The quasiparticle Green's function in the vicinity of the Fermi surface [$|\xi| \ll E_F$ and $|k - k_F(\hat{k})| \ll k_F(\hat{k})$] takes on the form:

$$G(\mathbf{k}, \xi) \approx \frac{z(\hat{k})}{i\xi - \mathbf{v}_F(\hat{k}) \cdot [\mathbf{k} - \mathbf{k}_F(\hat{k})]}, \quad (2)$$

where \mathbf{k} is the momentum and ξ is the Matsubara frequency, and the Fermi surface is parameterized in terms of the Fermi momentum $\mathbf{k}_F(\hat{k})$ in the direction of \hat{k} , with $\mathbf{v}_F(\hat{k})$ and $z(\hat{k})$ being the Fermi velocity and quasiparticle residue respectively. The Cooper instability then develops logarithmically slowly in the FL state and is marked by divergence of pairing susceptibility at the transition tem-

perature T_c that is exponentially small compared to the FL energy scale.

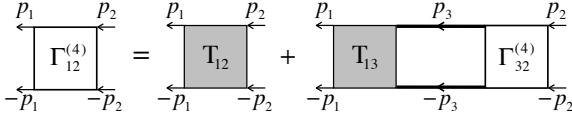


Fig. 3: Bethe-Salpeter equation for $\Gamma^{(4)}$, where $p_i \equiv (\xi_i, \mathbf{k}_i)$.

Physically, this behavior is typical for models with local repulsive coupling, where weak attractive effective interactions—described by the irreducible (in the particle-particle channel) four-pole vertex T —are an emergent low-energy property. By definition, T is the sum of all four-pole diagrams that can not be split into disconnected pieces by cutting two particle lines. From the Bethe-Salpeter relation, Fig. 3, for the full four-pole vertex $\Gamma^{(4)}$, we see that the smallness of the attractive part of T is a natural condition preventing $\Gamma^{(4)}$ from dramatic growth at $T \ll E_F$. Indeed, in the FL state, the leading contribution to the integral over \mathbf{k}_3 in the second term in the r.h.s. of Fig. 3 comes from $\int d^d k_3 \sum_{\xi_3} G(p_3)G(-p_3)$ in close vicinity to the Fermi surface, where only the finite temperature (i.e., discreteness of Matsubara frequency ξ_3) prevents it from logarithmic divergence. With the logarithmic accuracy at $T \ll E_F$, we have

$$\Gamma_{\hat{k}_1, \hat{k}_2}^{(4)} \approx T_{\hat{k}_1, \hat{k}_2} + \ln \frac{E_F}{T} \int T_{\hat{k}_1, \hat{k}_3} Q_{\hat{k}_3} \Gamma_{\hat{k}_3, \hat{k}_2}^{(4)} d^{d-1} \hat{k}_3, \quad (3)$$

where $\Gamma_{\hat{k}_1, \hat{k}_2}^{(4)}$ and $T_{\hat{k}_1, \hat{k}_2}$ are $\Gamma^{(4)}$ and T at vanishing frequencies projected to the Fermi surface:

$$\Gamma_{\hat{k}_1, \hat{k}_2}^{(4)} \equiv \Gamma^{(4)}(\mathbf{k}_1 = \mathbf{k}_F(\hat{k}_1), \xi_1 \rightarrow 0; \mathbf{k}_2 = \mathbf{k}_F(\hat{k}_2), \xi_2 \rightarrow 0),$$

and $Q_{\hat{k}}$ is the product of $z^2(\hat{k})$ and the single-component density of states at the \hat{k} -point on the Fermi surface. The systematic error in (3) comes from the ultra-violet cutoff scale, $E_F \rightarrow cE_F$, where c is some order-unity factor [33].

Switching to the matrix notations, $\Gamma_{\hat{k}_1, \hat{k}_2}^{(4)} \rightarrow \hat{\Gamma}^{(4)}$, $T_{\hat{k}_1, \hat{k}_2} \rightarrow \hat{T}$, $T_{\hat{k}_1, \hat{k}_2} Q_{\hat{k}_2} \rightarrow \hat{M}$, we find

$$\hat{\Gamma}^{(4)} \approx \left[1 - \ln(E_F/T) \hat{M} \right]^{-1} \hat{T}, \quad (4)$$

implying that $\Gamma^{(4)}$ —and thus the static response function in the Cooper channel—diverges at the critical temperature

$$T_c = c E_F e^{-1/\lambda}, \quad (5)$$

where λ is the largest positive eigenvalue of \hat{M} . The consistency of the emergent BCS picture based on weak Cooper instability requires $\lambda \ll 1$.

Solving the problem with logarithmic accuracy amounts then to finding the eigenvalues/eigenvectors of a real symmetric matrix

$$\mathcal{T}_{\hat{k}, \hat{k}'} \psi_{\hat{k}'} = \lambda \psi_{\hat{k}}, \quad \mathcal{T}_{\hat{k}, \hat{k}'} = Q_{\hat{k}}^{\frac{1}{2}} T_{\hat{k}, \hat{k}'} Q_{\hat{k}'}^{\frac{1}{2}}, \quad (6)$$

where the eigenvector $\psi_{\hat{k}}$ is the wave function of the Cooper pair in the momentum representation.

Parameterization and D_{4h} nomenclature in 2D. In two dimensions, it is convenient to parameterize \hat{k} with the polar angle θ , and to write the eigenvalue/eigenvector problem explicitly as

$$\int_0^{2\pi} \mathcal{T}_{\theta, \theta'} \psi_{\theta'} \frac{d\theta'}{2\pi} = \lambda \psi_{\theta}, \quad \mathcal{T}_{\theta, \theta'} = Q_{\theta}^{\frac{1}{2}} T_{\theta, \theta'} Q_{\theta'}^{\frac{1}{2}}, \quad (7)$$

$$Q_{\theta} = k_F(\theta) z^2(\theta) / [2\pi \hat{\theta} \cdot \mathbf{v}_F(\theta)]. \quad (8)$$

By the D_{4h} symmetry of the square lattice, $\mathcal{T}_{\theta, \theta'}$ splits into five independent blocks corresponding to s , p , $d_{x^2-y^2}$, d_{xy} , and g eigenvector sectors. The p -sector is doubly degenerate and can be further split into two independent sectors, p_x and p_y , related to each other by $\pm\pi/2$ rotations. For each of the six (sub)sectors, the symmetry properties of the corresponding vectors $f(\theta)$ are readily seen from their Fourier expansions (m is integer):

$$\begin{aligned} f_s(\theta) &= \sum_{m=0}^{\infty} A_m \cos(4m\theta), \\ f_g(\theta) &= \sum_{m=1}^{\infty} B_m \sin(4m\theta), \\ f_{\left\{ \begin{smallmatrix} p_y \\ p_x \end{smallmatrix} \right\}}(\theta) &= \sum_{m=0}^{\infty} C_m \left\{ \begin{array}{l} \cos[(2m+1)\theta] \\ \sin[(2m+1)\theta] \end{array} \right\}, \\ f_{\left\{ \begin{smallmatrix} d_{x^2-y^2} \\ d_{xy} \end{smallmatrix} \right\}}(\theta) &= \sum_{m=0}^{\infty} \left\{ \begin{array}{l} D_m \cos[(4m+2)\theta] \\ E_m \sin[(4m+2)\theta] \end{array} \right\}. \end{aligned} \quad (9)$$

The f_s is invariant with respect to all point-group operations; f_g is invariant with respect to $\pi/2$ rotations, but changes its sign under each of the four D_{4h} reflections; f_{p_y}/f_{p_x} is symmetric with respect to reflections over the x/y -axis and anti-symmetric with respect to reflections over the y/x -axis (also, the $\pi/2$ rotation of f_{p_y} turns it into f_{p_x}). The functions in both d sectors change their sign when rotated by $\pi/2$: $f_{d_{x^2-y^2}}/f_{d_{xy}}$ is symmetric/anti-symmetric with respect to reflections over x and y axes, and anti-symmetric/symmetric with respect to reflections by $\pm\pi/4$ axes. Fermionic anti-symmetry implies a spin-triplet state for p -wave pairing and a spin-singlet state for the other four sectors.

BDMC method with the ladder-summation trick. Similar to the system of resonant fermions, the locality of interaction allows one to introduce propagators based on interaction vertexes and pairs of fermions (and to fully dress them) by considering sums of ladder diagrams, see Ref. [30] and Fig. 4. Effectively, this amounts to replacing the bare interactions in Feynman diagrams with exact two-body scattering amplitudes; this trick is particularly important for dealing with strong interaction in the dilute gas limit by eliminating the expansion in a large parameter.

There is, however, a technical difficulty in combining bare interaction with ladder terms in the imaginary time

representation: The first term in the r.h.s. of Fig. 4 is a generalized $-U\delta(\tau)$ function (for resonant fermions, this term vanishes upon taking the zero-range limit), while the rest of the diagrams, $\tilde{\Gamma}$, is a continuous function of τ . The effective smallness of Γ in the dilute-gas regime at large $|U|$ takes place only under τ -integration and mathematically happens as follows. For large but finite U the sum of ladder diagrams behaves as a regularized $U\delta(\tau)$ function; i.e., the range of variation of $\tilde{\Gamma}(\tau)$ is $\sim 1/U$ while its amplitude is such that $\int_0^{\tau_0} \tilde{\Gamma}(\tau) d\tau \approx U$ for $\tau_0 \gg 1/|U|$. In Monte Carlo methods, however, the integration is achieved by sampling the *integrands* with the weighting factors proportional to their absolute values, meaning that a naïve scheme will sample $-U\delta(\tau)$ terms separately from $\tilde{\Gamma}(\tau)$ terms and their mutual compensation will be revealed only in the painful statistical limit.

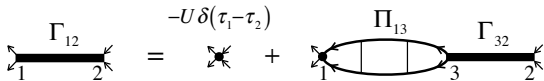


Fig. 4: The Γ -line in the time-momentum representation (spin and momentum indexes are suppressed for clarity): $\Gamma_{12} \equiv \Gamma(\tau_1 - \tau_2)$, $\Pi_{13} \equiv \Pi(\tau_1 - \tau_3)$, etc. Integration over internal times is assumed. Pair self-energy Π_{13} is the sum of all vertex-irreducible diagrams starting, at time τ_3 , and ending, at time τ_1 , with spin-up and spin-down outgoing (incoming) single particle propagators. A diagram is vertex-irreducible if it remains connected after cutting across any single interaction vertex. The lowest-order diagram contributing to Π_{13} is a pair of dressed propagators going from τ_3 to τ_1 . The second term in the r.h.s. is a continuous function of τ and will be referred to as $\tilde{\Gamma}$. Hence, $\Gamma(\tau, \mathbf{k}) = -U\delta(\tau) + \tilde{\Gamma}(\tau, \mathbf{k})$.

The solution is to transform the functional form of the bare vertex to make it (i) compatible with that of $\tilde{\Gamma}(\tau)$ at the level of *integrands*, and (ii) such that the diagram value remains intact under integration. To this end we introduce a function $\tilde{\Gamma}_U$ with the following properties

$$\int_0^\beta \tilde{\Gamma}_U(\tau) d\tau = -U. \quad (10)$$

The particular design of $\tilde{\Gamma}_U(\tau)$ still has a freedom. We choose $\tilde{\Gamma}_U(\tau) = -\tilde{\Gamma}(\tau) + c_0$, where c_0 is a constant of order unity or much smaller. This guarantees that, for $|U| \gg 1$, the condition of compensation, $\tilde{\Gamma}_U(\tau) \approx -\tilde{\Gamma}(\tau)$, is satisfied.

We then formally—and identically—represent each coupling constant U in the diagrammatic series as an integral over the auxiliary time variable associated with the bare vertex, thereby replacing the bare vertex with the $\tilde{\Gamma}_U$ function as pictured graphically in Fig. 5. Since $\tilde{\Gamma}_U$ has the same functional structure as $\tilde{\Gamma}$, we sum up the two elementary diagrammatic contributions into one, A_{1234} , as shown in Fig. 5. Thereby, we arrive at the diagrammatic formulation identical to that for resonant fermions [30],

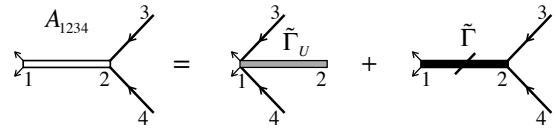


Fig. 5: The compensation trick. The diagram element A_{1234} is understood as the sum of two terms with different assignment of the end point for incoming fermionic propagators.

but with a modified rule for reading the diagram value: The single diagram element A_{1234} , now contributes a factor (momenta are suppressed for clarity)

$$A_{1234} = \tilde{\Gamma}_U(\tau_1 - \tau_2) G_\uparrow(\tau_1 - \tau_3) G_\downarrow(\tau_1 - \tau_4) + \tilde{\Gamma}(\tau_1 - \tau_2) G_\uparrow(\tau_2 - \tau_3) G_\downarrow(\tau_2 - \tau_4), \quad (11)$$

to the integrand of the diagram it enters. It contains two terms that become close in absolute values and opposite in sign when $|\tau_1 - \tau_2| \lesssim 1/|U|$. This is how the large- U compensation is achieved at the level of integrands. Apart from this specific way of evaluating the diagram value, the rest of the BDMC protocol is essentially identical to that for resonant fermions [30].

Numeric analysis. We employ the following protocol dictated by FL physics. We start with the BDMC simulation of the single-particle Green's function at some temperature $T \ll E_F$, low enough for observing a sharp Fermi-step in the momentum distribution, and extract all quasiparticle FL parameters. We then use this Green's function to perform the BDMC simulation of the irreducible vertex $T_{\hat{k}_1, \hat{k}_2}$, extract eigenvalues/eigenfunctions for all Cooper channels by solving the eigenvalue problem (7), and locate the phase boundaries from points where λ for the two competing ground-state phases coincide. All simulations are performed with explicit truncation of diagrammatic series at some maximum order N . Extrapolation with respect to N brings the corresponding systematic error under control, see Fig. 2.

We repeat these simulations at different temperatures to ensure that final results are temperature-independent. To eliminate the slowly vanishing (and quite substantial in the $n \rightarrow 0$ limit) finite-temperature correction to $T_{\hat{k}_1, \hat{k}_2}$, we observe that the leading term in this correction comes from the second-order diagram and hence calculate the corresponding contribution (semi-analytically) directly at $T = 0$. In addition, we have verified that spin and density correlations (particle-hole channels) do not exhibit any flow towards instability at low temperature for ($n = 0.6$, $U = 4$).

Conclusion. —Within the diagrammatic framework based on the unbiased BDMC method and asymptotically exact (in the weak-effective-coupling limit) theory of Cooper instability in the Fermi-liquid state, we revealed a significant part of rich ground-state phase diagram of the

fermionic Hubbard model on the square lattice. Specifically, we addressed the region of moderate bare coupling $U/t \leq 4$ and filling $n < 0.7$, where the system was found to exhibit Landau Fermi-liquid behavior within a broad temperature interval between the Fermi energy E_F and the superfluid transition temperature $T_c \ll E_F$ —a signature of the (emergent) weak effective coupling in the Cooper channel. The main reason why our data are confined to $U \leq 4$ and $n < 0.7$ is the convergence of diagrammatic series; it becomes problematic outside this range of parameters.

* * *

We are grateful to Kris Van Houcke and Félix Werner for sharing their expertise in code development, and to A. Chubukov, M. Baranov, E. Gull, J. Gukelberger, and M. Troyer for valuable discussions. We thank X.-W. Liu for his participation in the study of convergence of skeleton series. This work was supported by the Simons Collaboration on the Many Electron Problem, National Science Foundation under the grant PHY-1314735, the MURI Program “New Quantum Phases of Matter” from AFOSR, and the Swiss National Science Foundation, NSFC Grant No. 11275185, CAS, and NKBRSC Grant No. 2011CB921300. We acknowledge the hospitality of Kavli Institute for Theoretical Physics China at Beijing.

REFERENCES

- [1] HUBBARD J., *Proc. R. Soc. Lond. A*, **276** (1963) 238.
- [2] ANDERSON P. W., *The Theory of Superconductivity in the High- T_c Cuprates* (Princeton Univ. Press, Princeton, New Jersey) 1997.
- [3] KÖHL M., MORITZ H., STÖFERLE T., GÜNTER K. and ESSLINGER T., *Phys. Rev. Lett.*, **94** (2005) 080403.
- [4] JÖRDENS R., STROHMAIER N., GÜNTER K., MORITZ H. and ESSLINGER T., *Nature*, **455** (2008) 204.
- [5] SCHNEIDER U., HACKERMÜLLER L., WILL S., BEST TH., BLOCH I., COSTI T. A., HELMES R. W., RASCH D. and ROSCH A., *Science*, **322** (2008) 1520.
- [6] KAGAN M. Y. and CHUBUKOV A. V., *JETP Lett.*, **50** (1989) 517.
- [7] BARANOV M. A. and KAGAN M. Y., *Z. Phys. B: Condens. Matter*, **86** (1992) 237.
- [8] CHUBUKOV A. V. and LU J. P., *Phys. Rev. B*, **46** (1992) 11163.
- [9] CHUBUKOV A. V., *Phys. Rev. B*, **48** (1993) 1097.
- [10] ZANCHI D. and SCHULZ H. J., *Phys. Rev. B*, **54** (1996) 9509.
- [11] HALBOTH C. J. and METZNER W., *Phys. Rev. Lett.*, **85** (2000) 5162.
- [12] FUKAZAWA H. and YAMADA K., *J. Phys. Soc. Jpn.*, **71** (2002) 1541.
- [13] HLUBINA R., *Phys. Rev. B*, **59** (1999) 9600.
- [14] BLANKENBECLER R., SCALAPINO D. J. and SUGAR R. L., *Phys. Rev. D*, **24** (1981) 2278.
- [15] STAUDT R., DZIERZAWA M. and MURAMATSU A., *Eur. Phys. J. B*, **17** (2000) 411.
- [16] KOZIK E., BUROVSKI E., SCAROLA V. W. and TROYER M., *Phys. Rev. B*, **87** (2013) 205102.
- [17] WHITE S. R., *Phys. Rev. Lett.*, **69** (1992) 2863.
- [18] METZNER W. and VOLLHARDT D., *Phys. Rev. Lett.*, **62** (1989) 324.
- [19] GEORGES A. and KOTLIAR G., *Phys. Rev. B*, **45** (1992) 6479.
- [20] GEORGES A., KOTLIAR G., KRAUTH W. and ROZENBERG M. J., *Rev. Mod. Phys.*, **68** (1996) 13.
- [21] MAIER T., JARRELL M., PRUSCHKE T. and HETTLER M. H., *Rev. Mod. Phys.*, **77** (2005) 1027.
- [22] TOSCHI A., KATANIN A. A. and HELD K., *Phys. Rev. B*, **75** (2007) 045118.
- [23] RUBTSOV A. N., KATSNELSON M. I. and LICHTENSTEIN A. I., *Phys. Rev. B*, **77** (2008) 033101.
- [24] YANG S.-X., FOTSO H., SU S.-Q., GALANAKIS D., KHATAMI E., SHE J.-H., MORENO J., ZAAANEN J. and JARRELL M., *Phys. Rev. Lett.*, **106** (2011) 047004.
- [25] CHEN K.-S., MENG Z. Y., PRUSCHKE T., MORENO J. and JARRELL M., *Phys. Rev. B*, **86** (2012) 165136.
- [26] CHEN K.-S., MENG Z. Y., YANG S.-X., PRUSCHKE T., MORENO J. and JARRELL M., *Phys. Rev. B*, **88** (2013) 245110.
- [27] GULL E., PARCOLLET O. and MILLIS A. J., *Phys. Rev. Lett.*, **110** (2013) 216405.
- [28] ABRIKOSOV A. A., GOR'KOV L. P. and DZYALOSHINSKI I. E., *Methods of Quantum Field Theory in Statistical Physics* (Dover Publications, New York,) 1975.
- [29] GOR'KOV L. P. and MELIK-BARKHUDAROV T. K., *Sov. Phys. JETP*, **13** (1961) 1018.
- [30] VAN HOUCKE K., WERNER F., KOZIK E., PROKOF'EV N., SVISTUNOV B., KU M., SOMMER A., CHEUK L. W., SCHIROTZEK A. and ZWIERLEIN M. W., *Nature Physics*, **8** (2012) 366.
- [31] VAN HOUCKE K., WERNER F., PROKOF'EV N. V. and SVISTUNOV B. V., *arXiv:1305.3901*, (2013) .
- [32] KOZIK E., FERRERO M. and GEORGES A., *Phys. Rev. Lett.*, **114** (2015) 156402.
- [33] Methods for systematic (in parameter $g \ll 1$) evaluation of c are well-known [29] and will be discussed elsewhere.
- [34] In terms of the expansion (9), the nodal structure of the p -wave state is dominated by $\cos[\theta]$, while the nodal structure of the p' -eigenvector comes from $\cos[3\theta]$, rendering it akin to the f -wave state in continuous space.
- [35] RAGHU S., KIVELSON S. A. and SCALAPINO D. J., *Phys. Rev. B*, **81** (2010) 224505.
- [36] FERRERO M., *private communication*, (2014) .
- [37] OTSUKI J., HAFERMANN H. and LICHTENSTEIN A. I., *Phys. Rev. B*, **90** (2014) 235132.
- [38] SCHÄFER T., GELES F., ROST D., ROHRINGER G., ARRIGONI E., HELD K., BLÜMER N., AICHHORN M. and TOSCHI A., *Phys. Rev. B*, **91** (2015) 125109.
- [39] PHILLIPS P. AND DALIDOVICH D., *Phys. Rev. B*, **65** (2002) 081105(R).
- [40] DENG Y., KOZIK E., PROKOF'EV N. V. and SVISTUNOV B. V., *in progress*, (2015) .